



1 Evaluation of open and closed path sampling systems for determination 2 of emission rates of NH₃ and CH₄ with inverse dispersion modelling

3 Yolanda Maria Lemes^a, Christoph Häni^b, Jesper Nørlem Kamp^a, Anders Feilberg^{*a}

4 ^aDepartment of Engineering, Aarhus University, Gustav Wieds Vej 10D, 8000 Aarhus, Denmark.

5 ^bSchool of Agricultural, Forest and Food Sciences, Bern University of Applied Sciences, Länggasse 85, 3052
6 Zollikofen, Switzerland

7 **Corresponding author: email: af@bce.au.dk; Telephone: +45 30896099*

8 Declaration of interest: none

9 Abstract

10 The gas emission rates of ammonia (NH₃) and methane (CH₄) from an artificial source covering a surface
11 area of 254 m² were determined by inverse dispersion modelling (IDM) from point and line-integrated
12 concentration measurements with closed and open-path analyzers. Eight controlled release experiments
13 were conducted with different release rates ranging from 3.8 ± 0.21 to 17.4 ± 0.4 mg s⁻¹ and from 30.7 ±
14 1.4 to 142.8 ± 2.9 mg s⁻¹ for NH₃ and CH₄, respectively. The distance between the source and
15 concentration measurement positions ranged from 15 m to 60 m. Our study consisted of more than 200
16 fluxes averaged intervals of 10 min or 15 min. The different releases cover a range of different climate
17 conditions: cold (< 5°C), temperate (< 13 °C) and warm (< 18 °C). As the average of all releases with all
18 instrument types, the CH₄ recovery rate Q_{bLS}/Q was 0.95 ± 0.08 (n = 19). There was much more variation
19 in the recovery of NH₃, with an average of 0.66 ± 0.15 (n = 10) for all the releases with the line-integrated
20 system. However, with an improved sampling line placed close to the source an average recovery rate of
21 0.82 ± 0.05 (n = 3) was obtained for NH₃. Under comparable conditions, the recovery rate obtained with
22 an open-path analyzer was 0.91 ± 0.07 (n = 3). The effects of measurement distance, physical properties
23 of the sampling line, and deposition are discussed.

24 **Keywords:** Method validation, Ammonia, Methane, Inverse Dispersion Method, Backward Lagrangian
25 Stochastic, bLS



26 **1 Introduction**

27 The global agricultural system is currently facing one of its biggest humanitarian challenges:
28 feeding the world's rising population while preserving the environment and climate for future generations
29 (FAO, 2017). The agricultural sector is a major contributor to global greenhouse gas (GHG) emissions
30 (15%) and ammonia (NH₃) emissions (64%) (OECD and FAO, 2019), leading to air pollution, climate
31 change, deforestation, and loss of biodiversity (Aneja et al., 2009).

32 The European Union has established a reduction target for 2030 to reduce the GHG emissions by at
33 least 55% (EEA, 2019), compared to 1990, and NH₃ emissions by 19% (NEC Directive 2016/2284),
34 compared to 2005. Agriculture must contribute to GHG emission reductions, and valid estimates of GHG
35 emissions are important for national inventories regulation strategies and for selecting efficient mitigation
36 techniques.

37
38 Choosing the appropriate methodology to quantify gaseous emissions can be a challenge. In
39 particular agricultural sources are challenging as the sources often are small and inhomogeneous, exhibit
40 non-steady emissions over time (e.g. NH₃ emissions after slurry application (Hafner, 2018)) and are
41 influenced by other sources in close vicinity. Most of the methodologies have restrictions on the
42 measurement location and/or the source and involve complex instrumentation set-up (e.g., fast-response
43 analyzers, measurements at multiple heights). The micrometeorological mass balance (MMB) method
44 (Desjardins et al., 2004) requires measuring concentration at multiple positions several meters above the
45 ground, which is a challenge for obtaining high time resolution and it ignores the horizontal turbulent
46 transport (Hu et al., 2014). The tracer flux ratio method (TRM), which has also been used to measure
47 agricultural emissions (Vechi et al., 2022; Fredenslund et al., 2019; Delre et al., 2018), is a relatively
48 labor and cost intensive method typically with short intense measurement periods. In case of dynamic
49 emissions, this is not sufficient for resolving the temporal variations in emissions over days or weeks.



50 The inverse dispersion method (IDM) based on backward Lagrangian Stochastic (bLS) dispersion
51 modelling (e.g. Flesch et al., 2004, 1995) has been widely used for the assessment of NH₃ and methane
52 (CH₄) emissions from many agricultural sources: dairy housing (Bühler et al., 2021; VanderZaag et al.,
53 2014; Harper et al., 2009), cattle feedlot (McGinn et al., 2019; Todd et al., 2011; van Haarlem et al.,
54 2008; Flesch et al., 2007; McGinn et al., 2007), application of liquid animal manure (Kamp et al., 2021;
55 Carozzi et al., 2013; Sintermann et al., 2011; Sanz et al., 2010), grazed pasture (McGinn et al., 2011;
56 Voglmeier et al., 2018), rice field (Yang et al., 2019), lagoon (Ro et al., 2014; Wilson et al., 2001),
57 composting stockpiles (Sommer et al., 2004), agricultural biodigester (Baldé et al., 2016b; Flesch et al.,
58 2011), farm (Flesch et al., 2005) and stored liquid manure (Lemes et al., 2022; Baldé et al., 2016a; Grant
59 et al., 2015; McGinn et al., 2008).

60 IDM has been tested in controlled release experiments with different conditions: ground level
61 source without obstacles (Flesch et al., 2014; McBain and Desjardins, 2005a; Flesch et al., 2004), ground
62 level source surrounded by a fence (Flesch et al., 2005; McBain and Desjardins, 2005a), elevated source
63 (Gao et al., 2008; McBain and Desjardins, 2005a), multiple emission sources (Hu et al., 2016; Ro et al.,
64 2011; Gao et al., 2008) and to quantify the effect of NH₃ deposition (Häni et al., 2018).

65 IDM is a function of the geometry and location of source and downwind concentration sensor
66 (including height for the sensor) and the turbulence characteristics in the surface layer. The statistical
67 properties of the flow in the atmospheric surface layer for the IDM are defined by the friction velocity
68 (u^*), roughness length (z_0), the Obukhov length (L), and wind direction (Flesch et al., 2004). Emissions
69 are derived from concentration measurements up- and downwind of the source, which could be
70 determined with point or line-integrated measurements from closed- or open-path analyzers. IDM
71 assumes an ideal atmospheric surface layer, which means i) a horizontally homogeneous and flat surface,
72 ii) homogeneity and quasi-stationarity with respect to the turbulence characteristics and iii) spatially
73 uniform emissions from a confined source (Flesch et al., 2004). Therefore, there should not be any
74 obstacles (e.g., trees, buildings) in close vicinity of the source to fulfil the required IDM assumptions.



75 Additionally, IDM has the limitation that there should not be any other sources of the same gas species
76 that affects up- and downwind concentration differently. The IDM is simple, flexible (Harper et al.,
77 2011), robust even in no ideal conditions and has a reported accuracy of $100 \pm 10\%$ when it is properly
78 used (e.g., place of instruments, filtering criteria) (Harper et al., 2010). Moreover, IDM is a direct
79 measurement method that does not alter the physical properties of the source, and it is applicable for both
80 small and large emissions of any shape of sources (Flesch et al., 2004) as opposed to indirect enclosure
81 methods (e.g. chambers measurements).

82 Concentration measurements are mostly done with an open-path optical system (e.g. Baldé et al.,
83 2018; Bühler et al., 2021) because long path lengths (>50 m) enable a higher emission plume coverage
84 and avoids internal surfaces (e.g. tubes, pumps) where NH_3 can adsorb (Shah et al., 2006; Vaattinen et al.,
85 2014). However, open-path has a limitation on low concentration measurements (<10 ppb for CH_4 and
86 NH_3) (Bai et al., 2022) and requires complex calibrations to reduce the uncertainty of the measurements
87 (Häni et al., 2021; DeBruyn et al., 2020). In addition, it requires intensive labor to move and optically
88 align the instruments to different positions depending on the predominant wind direction. Commercially
89 available open-path analyzers exhibit limitations with respect to acceptable detection limits (Häni et al.,
90 2021). Closed-path analyzers have rarely been used together with the IDM (Ro et al., 2011) due to its
91 limitation caused by adsorption of NH_3 in the system. In addition, closed path analyzers have only been
92 used for point measurements, which challenges the ability to catch the emission plume and makes it
93 sensitive to wind direction accuracy.

94 Data filtering is needed to ensure accuracy of the IDM, which is related to the meteorological
95 conditions (e.g., wind speed, atmospheric stability) and wind direction. The quality criteria for filtering
96 are based on the atmospheric conditions in a measurement interval to ensure the assumptions of the model
97 is adequately meet, which also lower the uncertainty of the resulting data. Different criteria have been
98 used in previous studies: Flesch et al. (2005) recommend to remove data where $u^* < 0.15 \text{ m s}^{-1}$, $|L| < 10 \text{ m}$
99 and $z_0 > 1 \text{ m}$, whereas McBain and Desjardins, 2005 recommend $u^* < 0.19 \text{ m s}^{-1}$, $|L| \leq 3 \text{ m}$ and $z_0 > 1 \text{ m}$.



100 Flesch et al. (2014) suggest the filtering criteria for the night of $u^* < 0.05 \text{ m s}^{-1}$ and the gradient between
101 measured and MO-calculated temperature ($|\Delta\Delta T|_{\text{thres}} = 0.05 \text{ K}$. Bühler et al. (2021) removed data
102 where $u^* < 0.05 \text{ m s}^{-1}$, $|L| < 2 \text{ m}$, $z_0 > 0.1 \text{ m}$, standard deviation of the horizontal wind components (u, v)
103 divided by $u^*(\sigma_{u,v}/u^*) > 4.5$ and Kolmogorov constant (C_0) > 10 .

104 This study aimed to assess the applicability and performance of a closed-path analyzer used with a
105 sampling system that allows for line integrated concentration measurements used with the IDM for
106 determining emission rates of CH_4 and NH_3 . This novel measuring system will allow for measuring
107 emissions from sources with low emission rates and will have good flexibility for moving it around the
108 source depending on the wind direction in order to increase the probability of catching the emission
109 plume. This novel method is assessed by eight controlled releases of CH_4 and NH_3 combined with up- and
110 downwind measurements in different positions using point and line-average concentration provided with
111 closed- and open-path analyzers. The use of CH_4 and NH_3 and open- and closed-path systems to measure
112 concentration will give us an opportunity to: i) test the system of the line-average concentration
113 measurement with a closed-path analyzer; and ii) evaluate potential loss of NH_3 downwind from the
114 source by deposition and/or gas-to-particle conversion, processes that will not occur for inert CH_4 . This
115 controlled-release study is the first to compare the performances of open-path and line-integrated closed-
116 path systems for measuring emissions of NH_3 and CH_4 .

117

118 **2 Material and methods**

119 **2.1 Site descriptions**

120 From November 2019 to March 2022, eight controlled release experiments were performed at
121 different grassland sites under varying conditions (see Table 1). Five releases (I-DK to IV-DK and VIII-
122 DK) took place at AU campus Viborg, Denmark on two different fields ($56^\circ 29' 34.5'' \text{N} / 9^\circ 34' 28.3'' \text{E}$ and
123 $56^\circ 29' 36.4'' \text{N} / 9^\circ 34' 15.9'' \text{E}$). Three releases (V-CH to VII-CH) were performed at Bern University of



124 Applied Sciences, Switzerland (46°59'35.1"N / 7°27'43.1"E). At all sites, the terrain was horizontally flat,
125 and the height of the canopy varied between 15 and 25 cm for the different experiments. Obstacles upwind
126 of the artificial source were more than 100 m away in all experiments. There were no significant sources
127 near the experiment sites.

128 2.2 Instrumentation

129 In this study, different models of cavity ring-down spectroscopy (CRDS) from Picarro (Picarro Inc.,
130 Santa Clara, CA, USA) were used to measure up- and downwind NH₃ and CH₄ concentration (Table 1).
131 Model G2201-i and model G4301 measure CH₄ concentration, G2103 measures NH₃ concentration, and
132 G2509 measures CH₄ and NH₃ simultaneously. The CRDS is a closed-path analyzer with continuous
133 absorption that measure concentrations at approximately 0.5 Hz. The CRDS analyzer consists of a laser and
134 an optical cavity chamber with highly reflective mirrors, which gives an effective path length of several
135 kilometers. The light is absorbed in the cavity, and the decay of light intensity is called the ring-down time,
136 which is directly related to the concentration of the specific compound. It has been frequently used to study
137 agricultural emissions (e.g., Kamp et al., 2021; Pedersen et al., 2020; Kamp et al., 2019; Sintermann et al.,
138 2011).

139 In experiments V-CH to VII-CH, the downwind CH₄ concentration was measured with three
140 GasFinder3 analyzers (GF3, Boreal Laser Inc., Edmonton Canada) and the downwind NH₃ concentration
141 with three miniDOAS instruments (Sintermann et al., 2016). The GF3 analyzer is an open-path tunable
142 diode laser device that measures line-integrated CH₄ concentrations over path lengths of 5 to 500 m (i.e.
143 single path length between sensor and retroreflector) with a temporal resolution of 0.3 to 1 Hz. The
144 retroreflectors used in the experiments were equipped with seven corner cubes, suitable for path lengths
145 around 50 m. The GasFinder devices have been widely used to measure emissions from different type of
146 agricultural sources with the IDM (Bühler et al., 2021; McGinn et al., 2019; VanderZaag et al., 2014; Harper
147 et al., 2010; Flesch et al., 2007). The performance of the GF3 instruments is discussed in detail by Häni et
148 al. (2021).



149 The miniDOAS instrument is an open-path device that measures NH₃, NO and SO₂ in the UV region
150 between 190 and 230 nm based on the differential optical absorption spectroscopy (DOAS; Platt and Stutz,
151 2008) technique. It provides path-averaged concentrations for path lengths between 15 m and 50 m, with
152 around 10 to 20 scans per second averaged over 1 minute. Ammonia emissions from agricultural sources
153 (Kamp et al., 2021; Kupper et al., 2021; Voglmeier et al., 2018) and from an artificial source (Häni et al.,
154 2018) have been measured with miniDOAS analyzers. Further details on the instrument is given in
155 Sintermann et al. (2016).

156 2.3 Gas release from an artificial source

157 The artificial source area had a gas distributor unit at the center and eight 1/4" polytetrafluoroethylene
158 (PTFE) tubes leave the distributor to get a circular shape of the source area. Each tube contained three
159 critical orifices (100 µm diameter, stainless steel, LenoxLaser, USA) in series with 3 m distance between
160 them. In total, the 24 orifices covered a circular area of 254 m².

161 Gas was released from a gas cylinder and the flow was controlled with a mass flow controller (in
162 Denmark: Bronkhorst EL FLOW, Ruurlo, Netherlands; in Switzerland: red-y smart controller, Voegtlin
163 Instruments GmbH, Aesch, Switzerland). The source height, the content of the gas cylinders, and the release
164 rate for each experiment are given in Table 1.

165

166

167



168 **Table 1** Date, gas cylinders description, ammonia and methane release rate (RR), source and canopy height, downwind
 169 distance from source to instruments, type of system attached to the cavity ring-down spectroscopy (CRDS), and
 170 instrumentation of each controlled release experiment (CRE). G2103, G2202-i, G4301 and G2508 are different CRDS
 171 models, GF correspond to GasFinder and MD to miniDOAS.

CRE	Date	Gas cylinder			NH ₃ RR [mg s ⁻¹]	CH ₄ RR [mg s ⁻¹]	Source height [cm]	Canopy height [cm]	Distance from source edge [m]	System with CRDS	Instruments
		Content	[bar]	total							
I- DK	29-11-2019 11:50 – 12:50	5% NH ₃ and 95% N ₂ ± 2%*	62	1	4.6 ± 0.3	-	0	20	50	Point 40°C	2 G2103
II- DK	29-11-2019 14:00-14:30	99% CH ₄ and 1% N ₂ ± 2%*	62	1	-	30.7 ± 1.4	0	20	50	Point 40°C	G2201-i and G4301
III- DK	12-10-2020 11:45-15:15	5% NH ₃ and 95% CH ₄ ± 2%*	62	1	3.8 ± 0.21	68.7 ± 3.7	0	25	35 - 60	16m line 40°C (Line 1)	G2103, G4301 and G2508
IV- DK	20-07-2021 10:30-16:00	10% NH ₃ and 90% CH ₄ ± 2%*	62	2	17.4 ± 0.4	142.8 ± 2.9	50	18	15-30	12m line 40°C (Line 2)	G2103, G4301 and G2508
V- CH	09-10-2021 10:00-12:10	10% NH ₃ and 90% CH ₄ ± 2% ⁺	27	2	15.2 ± 0.3	128.9 ± 2.7	0	15	15 - 30 - 60	16m line 40°C (Line 1)	G4301, G2508, 3 GF and 3 MD
VI- CH	09-10-2021 14:20-16:50	10% NH ₃ and 90% CH ₄ ± 2% ⁺	27	4	13.2 ± 0.3	111.8 ± 2.2	0	15	15 - 30 - 60	16m line 40°C (Line 1)	G4301, G2508, 3 GF and 3 MD
VII- CH	09-10-2021 17:20-17:50 11-10-2021 15:10-16:20	10% NH ₃ and 90% CH ₄ ± 2% ⁺	27	4	13.2 ± 0.3	111.8 ± 2.2	50	15	15 - 30 - 60	16m line 40°C (Line 1)	G4301, G2508, 3 GF and 3 MD
VIII- DK	22-04-2022 12:30-15:00	10% NH ₃ and 90% CH ₄ ± 2%*	62	2	14.5 ± 0.3	118.9 ± 2.8	50	7	15	12m line 40°C (Line 2)and 12m line 80°C with heated inlets (Line 3)	3 G2508

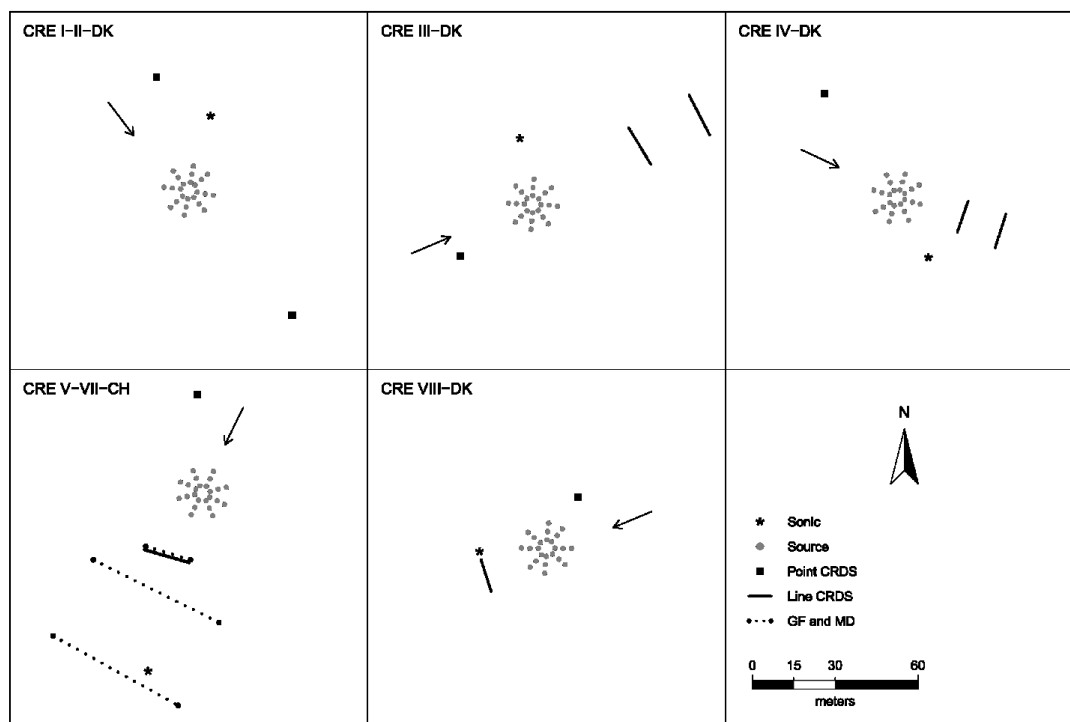
*Air Liquide, Horsens, Denmark
⁺Carbagas, Bern, Switzerland



173 2.4 Set-up

174 In the upwind position of all the experiments and in the downwind position of the I-DK and II-DK
175 experiment, the CRDS measured the concentration from a single point 1.5 m above ground through a
176 polytetrafluoroethylene (PTFE) tube that was insulated and heated to approximately 40°C. In the rest of the
177 experiments, the CRDS measured downwind concentration from a sampling line system of PTFE tubes
178 insulated and heated (40°C or 80°C). In the III-DK, V-DK, VI-CH, and VII-CH experiment, the sampling
179 line system consisted of a 16 m tube with nine inlets, 2 m between each inlet (Line 1). In the IV-DK and
180 VIII-DK experiment, the sampling lines were 12 m long with seven inlets, 2 m between each inlet (Line 2
181 and Line 3). The inlets are made of critical orifices (0.25 mm ID for I-DK to VII-CH and 0.5 mm ID for
182 VIII-DK polyetheretherketone (PEEK)) that guarantee uniform flow through each inlet (Line 1, Line 2 and
183 Line 3). In the VIII-DK experiment, the sampling line system including the inlets was heated to 80°C (Line
184 3).

185 Figure 1 shows the position of the source area relative to the sampling position and the arrow
186 indicates the wind direction during the experiments. The downwind concentration were measured in one,
187 two or three distance (Table 1). In the V-CH, VI-CH and VII-CH, downwind concentrations were measured
188 at the same time at 15 m, 30 m and 60 m distance from the edge of the source with multiple GF3 and
189 miniDOAS instruments; one CRDS instrument was placed 15 m downwind (Figure 1). The distance
190 between the reflector and the laser/detector of the GF3 and miniDOAS at the downwind position parallel
191 to the CRDS sampling line was also 16 m. For the other two downwind positions the path lengths were 15
192 m and 50 m, respectively. The height of the measurement paths of all the open-path instruments were
193 between 1.2 and 1.5 m. The background concentration of NH₃ was stable with no sources in close vicinity,
194 thus in the three experiments, the average concentration of each instrument 10 min before the release of
195 each experiment was used as the NH₃ upwind concentration for the miniDOAS and the CRDS instruments
196 . In the V-CH, VI-CH and VII-CH experiment the measured NH₃ background concentration was 2.7 and
197 4.1 mg m⁻³, and 2.1 and 4.8 mg m⁻³ for the miniDOAS and the CRDS, respectively.



198

199 *Figure 1 – Position of the orifices of the artificial source, ultrasonic anemometer (sonic), and the*
200 *concentration analyzer used in the eight controlled release experiments (CRE) of this study. Three*
201 *types of analyzers have been used: cavity ring-down spectrometer (CRDS), GasFinder (GF) and*
202 *miniDOAS (MD). The arrow indicates the wind direction during each experiment.*

203 In Denmark, the three wind components were measured at 16 Hz with a 3D ultrasonic anemometer
204 (WindMaster, Gill, Hampshire, UK) at 1.5 and 1.7 m height. In addition to concentration and wind, air
205 temperature, and atmospheric pressure were also measured. In Switzerland, the wind components were
206 measured at 20 Hz with a 3D ultrasonic anemometer (WindMaster, Gill, Hampshire, UK) at 2 m height.
207 Air temperature and atmospheric pressure were obtained from a meteorological station nearby the
208 experiment site.

209 A Global Positioning System (in Denmark: GPS Trimbel R10, Sunnyvale, California, USA; in
210 Switzerland: GPS Trimble Pro 6, Sunnyvale, California, USA) was used to record the position of all
211 instruments and the individual critical orifices of the source.



212 2.5 Inverse dispersion method

213 The measured gas emission rates (Q) from the artificial source were calculate in 15 min
214 (experiments conducted in Denmark) or 10 min average intervals (experiments conducted in Switzerland)
215 using the R (R Core Team, 2018) package bLSmodelR (<https://github.com/ChHaeni/bLSmodelR>;
216 version 4.3) as described by Häni et al. (2018). The simulation was performed with six million backward
217 trajectories (N) and the source area defined as 24 individual circles of 5 cm radius as described by Häni et
218 al. (2018) with a high performance computer cluster (PRIME - Programming Rig for Modern
219 Engineering, Aarhus University).

220 The emissions rate (Q) is proportional to the difference between measured concentration downwind
221 (C_{downwind}) from the source and the measured background concentration (C_{upwind}), and the dispersion
222 factor (D):

$$Q = \frac{C_{\text{downwind}} - C_{\text{upwind}}}{D} \quad (1)$$

223 The dispersion factor (D) is calculated as:

$$D = \frac{1}{N} \sum_{\text{TDinside}} \left| \frac{z}{w_{\text{TD}}} \right| \quad (2)$$

224 where N is the number of backward trajectories from the downwind analyzer location. The
225 summation refers to the trajectories touching inside the source area (TDinside) taking the vertical
226 velocity (w_{TD}) at touchdown into account. The calculation of D includes determination of wind profiles
227 and turbulence statistics that are based on the Monin-Obukhov Similarity Theory (MOST).

228 2.6 Surface deposition velocity

229 Ammonia is a relatively short lived gas in the atmosphere and can either be chemically converted, or
230 subjected to dry or wet deposition. The dry NH_3 deposition rate is usually expressed with a deposition
231 velocity (u_d^*). It is a complicated phenomenon that is controlled by both atmospheric and land surface



232 processes (e.g. wind speed, solar radiation, vegetation reactivity). In this study, we assume v_d takes place
233 uni-directionally and it is calculated with the canopy resistances:

$$v_d = \frac{1}{R_a + R_b + R_c} \quad (3)$$

234 where R_a is the aerodynamic resistance, R_b is the quasi-laminar boundary resistance and R_c is the bulk
235 canopy resistance. R_a is a function of wind speed and friction velocity (Baldocchi et al., 1987) that is
236 included in the bLS model, therefore Eq. 3 can be simplified as:

$$v_d^* = \frac{1}{R_b + R_c} \quad (4)$$

237 According to Garland (1977), R_b can be calculated with Eq. 5 as a function of the roughness length
238 (z_0), the friction velocity (u^*), the kinematic viscosity of air (ν) and the molecular diffusivity of NH_3 in
239 air (δ_{NH_3}).

$$R_b = \frac{1.45 \left(\frac{z_0 u^*}{\nu} \right)^{0.24} \left(\frac{\nu}{\delta_{\text{NH}_3}} \right)^{0.8}}{u^*} \quad (5)$$

240 Regarding R_c , it is related to the chemical characteristics of the studied gas and the characteristics of
241 the leaf (e.g. type, size). There are different models to calculate R_c . Due to the complexity and the
242 uncertainty of the determination of the resistance, R_c was calculated following the same procedure as by
243 Häni et al. (2018) with the bLSmodelR. It was assumed that $Q_{\text{bLS}}/Q < 1$ was solely due to dry deposition.
244 A similar approach is used here, where 12 values of R_c from 0 to 500 s m^{-1} were tested in the bLS model
245 that includes ammonia deposition to estimate the R_c giving $Q_{\text{bLS}}/Q = 1$ in all intervals. This was done with
246 linear interpolation between the two points closest to $Q/Q = 1$. Using this estimated R_c and the calculated
247 R_b value for each interval, v_d^* was estimated for all intervals with all instruments. The v_d^* values are
248 compared to previously reported values for NH_3 .



249 Another approach for calculating the R_c is with empirical equation, which will be used for calculating
250 values for v_d^* . These calculated values will be compared to the values obtained with the bLS model. It is
251 assumed that R_c unidirectional and equal to the sum of the stomatal resistance R_s and the cuticular
252 resistance R_w , see Eq.6.

$$\frac{1}{R_c} = \frac{1}{R_s} + \frac{1}{R_w} \quad (6)$$

253 The stomatal resistance R_s is calculated with equation Eq.7 (Wesely, 2007):

$$R_s = R_{s(\min)} \left[1 + \left(\frac{200}{SR + 0.1} \right) \right]^2 \frac{400}{T_s(40 - T_s)} \quad (7)$$

254 where $R_{s(\min)}$ is minimum bulk canopy R_s for water vapour that is assumed to be equals to 250 s
255 m^{-1} (Lynn and Carlson, 1990), SR is the solar radiation, and T_s is the soil temperature.

256 The cuticular resistance is calculated with Eq. 8 (Massad et al., 2010):

$$R_w = \frac{R_{w(\min)} e^{a(100-RH)} e^{0.15T}}{(LAI)^{0.5}} \quad (8)$$

257 where $R_{w(\min)}$ is the minimum cuticular resistance, a is an empirical factor, RH is the relative
258 humidity, T is the air temperature, and LAI is the leaf are index. The parameters $R_{w(\min)}$ ($10 s m^{-1}$), a
259 (0.110) and LAI ($2 m^2 m^{-2}$) were obtained from Massad et al., 2010, Table 1.

260 **3 Results and discussion**

261 3.1 Recovered fractions of Ammonia and Methane

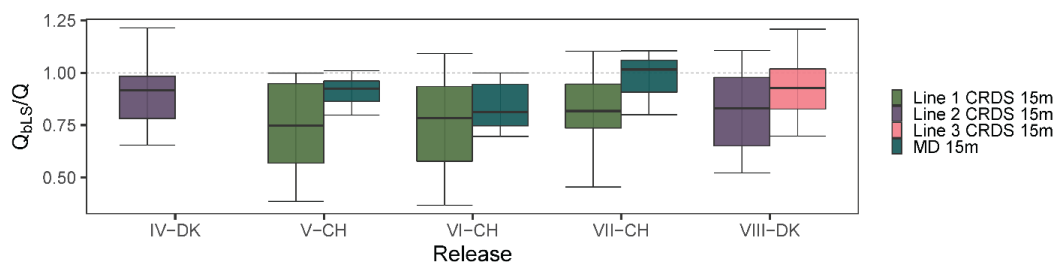
262 The accuracy of the bLS model is evaluated by the recovered NH_3 and CH_4 fractions, Q_{bLS}/Q , and
263 the standard deviation $\sigma_{Q_{bLS}/Q}$ (\pm) for all the releases. In all experiments except I-DK and II-DK (Table 1),
264 NH_3 and CH_4 were released simultaneously. The use of these two gases give us the additional opportunity



265 to assess potential loss of NH_3 downwind from the source by deposition or gas-to-particle conversion,
266 processes that will not occur for CH_4 due to its inertness. As the average of all releases and measurement
267 systems, the CH_4 recovery rate was 0.95 ± 0.08 ($n = 19$) (Figure 4). This recovery is similar to 0.93 ± 0.14
268 ($n = 8$) observed by Gao et al. (2008) with a different controlled releases configuration and ground-level
269 sources. There was more variation in the recovery of NH_3 , with an average of 0.66 ± 0.15 ($n = 10$) for all
270 the releases with the line-integrated system. However, the improved sampling lines (Line 2 and 3) placed
271 at 15 m downwind from the source had an average recovery of 0.82 ± 0.05 ($n = 3$) for NH_3 (Figure 2).
272 Under comparable conditions, the NH_3 recovery rate obtained with the miniDOAS (MD) was 0.91 ± 0.07
273 ($n = 3$). Häni et al. (2018) observed almost the same recovered fraction, 0.91 ± 0.12 , at 15 m from the
274 edge of the source with the MD. The recovery rates of all experiments in this study are shown in Figure 2,
275 Figure 3 and Figure 4, whereas climate conditions such as wind direction, friction velocity u_* , air
276 temperature, relative humidity (RH), soil temperature and solar radiation (SR) from each experiment are
277 presented in Table 2. I-DK and II-DK were conducted during cold conditions ($\sim 5^\circ\text{C}$) with RH ranging
278 from 65 % to 71 %, whereas IV-DK and VIII-DK were conducted in warm conditions (14 – 18°C) with
279 RH between 48 % and 63 %. The other releases were conducted under moderate temperature conditions
280 (10 – 13°C) with RH between 39% and 89%.

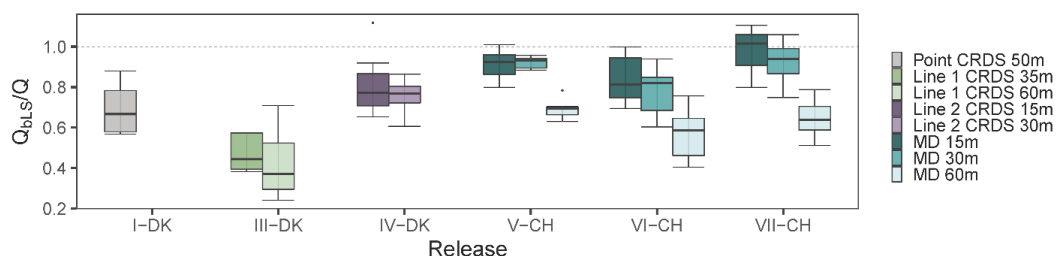
281 Additional information on the atmospheric conditions, weather conditions, and recovery fraction
282 rates for each average time interval for each release are shown in Table S1 in the Supplementary
283 Information.

284



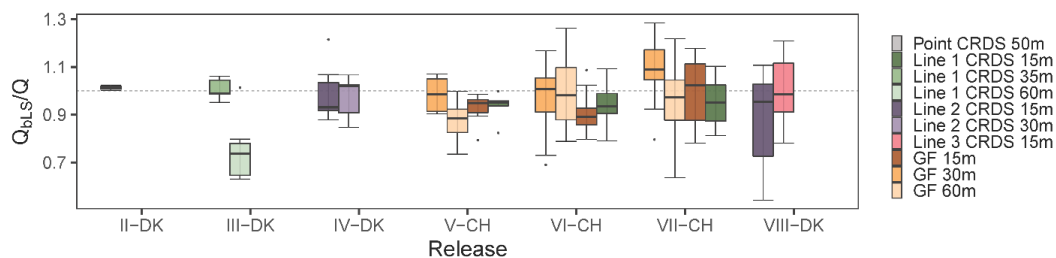
285
 286 *Figure 2 .- The recovered fractions Q_{bls}/Q of ammonia from the releases where line 1, 2 and 3, and*
 287 *miniDOAS (MD) are placed 15 m from the edge of the source. Line 1 had a length of 16 m, and it was*
 288 *heated to 40 °C. Line 2 had the same temperature as Line 1, but it was 12 m long. Line 3 had the same*
 289 *length as Line 2, but was heated to 80 °C.*

290



291
 292 *Figure 3 .- The recovered fractions Q_{bls}/Q of ammonia from the releases where point concentration*
 293 *measurement was used and where concentration downwind distance was measured in two or three*
 294 *distances from the edge of the source. Line 1, Line 2 and Line 3 are described in the Figure 2 caption.*

295



296
 297 *Figure 4 .- The recovered fractions Q_{bls}/Q of methane for each release and analyzer. The downwind*
 298 *distance from the source to the analyzer is indicated in the legend. Line 1, Line 2 and Line 3 are*
 299 *described in the Figure 2 caption.*

300



301 Table 2 – Atmospheric and weather conditions in terms of friction velocity (u^*), wind speed (WS), air
 302 temperature (T_{air}), air pressure (P_{air}), soil temperature (T_{soil}), solar radiation (SR) and relative humidity (RH)
 303 during each release of this study.

Release	u^* [m s ⁻¹]	WS [m s ⁻¹]	T_{air} [°C]	P_{air} [hPa]	T_{soil} [°C]	SR [W m ⁻²]	RH [%]
I-DK	0.23 ± 0.05	2.4 ± 0.5	4.5 ± 0.3	993.6 ± 0.3	5.5 ± 0.1	167.5 ± 34.4	69.6 ± 1.7
II-DK	0.19 ± 0.03	1.8 ± 0.1	4.8 ± 0.1	995.4 ± 0.1	5.6 ± 0.1	117.1 ± 8.4	64.7 ± 0.2
III-DK	0.22 ± 0.03	2.2 ± 0.3	11.7 ± 3.1	1005.3 ± 0.3	10.3 ± 0.2	139.5 ± 50.7	76.7 ± 1.3
IV-DK	0.45 ± 0.04	5.1 ± 0.5	17.9 ± 0.4	1009.1 ± 0.1	17.6 ± 0.2	378.8 ± 152.1	66.7 ± 2.4
V-CH	0.36 ± 0.03	4.5 ± 0.1	9.4 ± 0.3	958.9 ± 0.1	11.8 ± 0.0	238.3 ± 47.8	86.5 ± 1.7
VI-CH	0.20 ± 0.04	2.3 ± 0.4	11.1 ± 0.3	959.6 ± 0.0	12.7 ± 0.2	178.7 ± 41.4	75.5 ± 1.8
VII-CH	0.26 ± 0.08	3.2 ± 1.0	12.8 ± 0.9	959.4 ± 0.1	11.5 ± 0.9	340.8 ± 161.7	52.1 ± 13.2
VIII-DK	0.43 ± 0.05	4.7 ± 0.3	13.9 ± 0.6	1008.9 ± 0.2	8.7 ± 0.3	691.7 ± 53.2	51.4 ± 2.4

304

305 3.2 Sampling systems for closed-path measurement

306 Three different CRDS sampling line systems have been used from III-DK to VIII-DK. The difference
 307 between the lines was the length and the heating temperature. Line 1 had a length of 16 m, and it was heated
 308 to 40 °C. Line 2 had the same temperature as Line 1, but it was 12 m long. Line 3 had the same length as
 309 Line 2, but was heated to 80 °C, and the critical orifices have a higher inflow than Line 1 and Line 2 (see
 310 section 2.4 Set-up). We expect that decreasing the length and increasing the heating temperature of the line
 311 will improve Q_{bLS}/Q for NH_3 (no expected effect for CH_4) by avoiding adsorption and reducing the response
 312 time in the sampling line.

313 Line 1 was used with the source at ground level and elevated (Table 1), whereas the other two lines
 314 only with the source elevated. When the source was at ground level, Line 1 had a recovery rate ranging
 315 from 0.42 ± 0.17 to 0.60 ± 0.10 and from 0.75 ± 0.13 to 1.01 ± 0.05 for NH_3 and CH_4 , respectively. The
 316 lowest and the highest NH_3 recovery rate of Line 1 are directly related to the furthest (60 m) and the shortest
 317 (15 m) downwind distance measurement from the source. In addition, the standard deviation $\sigma_{Q_{\text{bLS}}/Q}$ at the
 318 furthest position is higher than at the closest position, which is in accordance with the results from Häni et
 319 al. (2018). High uncertainty of the Q_{bLS}/Q is related to a smaller difference in concentration between
 320 downwind and background concentrations and due to smaller D-values (Häni et al., 2018). This is also the



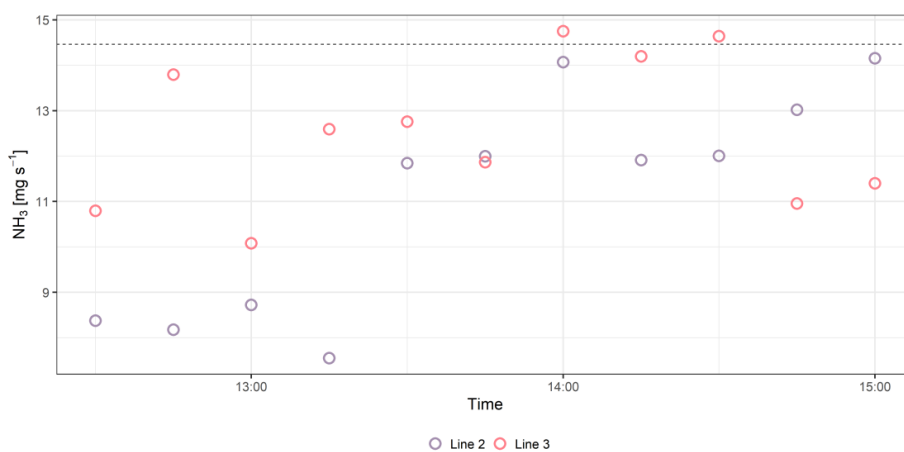
321 reason for the low CH₄ recovery rate of Line 1 in III-DK at 60 m (0.75 ± 0.13), downwind concentration is
322 only 4 – 10% higher than upwind concentrations since this is one of the lowest CH₄ releases rate (Table 1).
323 This is in line with Coates et al. (2021), who observed that the bLS model underestimated 49% of CO₂
324 released at 50 m fetch distance partially because the measured downwind concentration was close to the
325 background level. Therefore, in this study, the accuracy of Q_{bLS} is mainly influenced by the uncertainty of
326 the concentration measurement, hence the downwind distance is limited by the properties of the gas
327 analyzers and the size of the emission strength of the source. This means the system can be limited in use
328 if the emission source has a large height and low emission strength where, as a rule of thumb, measurements
329 should be conducted at a distance from the source at least 10 times the height of the source (Harper et al.,
330 2011).

331 In VII-CH, Line 1 was used with the source elevated and had a recovery rate of 0.69 ± 0.12 for NH₃
332 and 0.95 ± 0.10 for CH₄. Line 2 had a numerically higher recovery rate than Line 1, ranging from $0.76 \pm$
333 0.08 to 0.81 ± 0.16 and from 0.89 ± 0.20 to 0.99 ± 0.12 for NH₃ and CH₄, respectively in IV-DK and VIII-
334 DK. As expected, the lowest NH₃ recovery rate of Line 2 was at the furthest downwind measurement
335 position (30 m). The length of the line appears to affect the NH₃ recovery rate; this might be due to the
336 increased surface area that NH₃ can adsorb to stick, and there is a lower flow in each of the critical orifices
337 that decreases the response time of the system (Shah et al., 2006; Vaittinen et al., 2014). Looking at the
338 measured NH₃ rates over time (Figure 5), higher emissions are reached with Line 3 for the first hour
339 indicating a faster time response compared to Line 2. However, after an hour there was not a clear difference
340 between the lines. The results indicate that increasing the sampling line temperature to 80 °C had a positive
341 effect on the recovery, which reached 87 % at a distance of 15 m. From the data obtained by the open-path
342 analyzer (MD), we can conclude that deposition can cause a reduction in recovery in the order of 2-16%
343 (Figure 2). Thus, the recovery obtained with the improved line (Line 3) approaches the recovery obtained
344 with the open-path analyzer. It should be noted that a direct comparison between Line 3 and the open-path
345 analyzer (MD) has not been made and further improvement can still be suggested for the CRDS sampling



346 line system. Specifically, increasing the flow on the sampling line will reduce NH_3 adsorption in the tubing
347 material. This can be achieved by increasing the flow through the tubing and the critical orifices but
348 maintaining an even flow distribution through the discrete sampling inlets in the sampling line must still be
349 maintained.

350



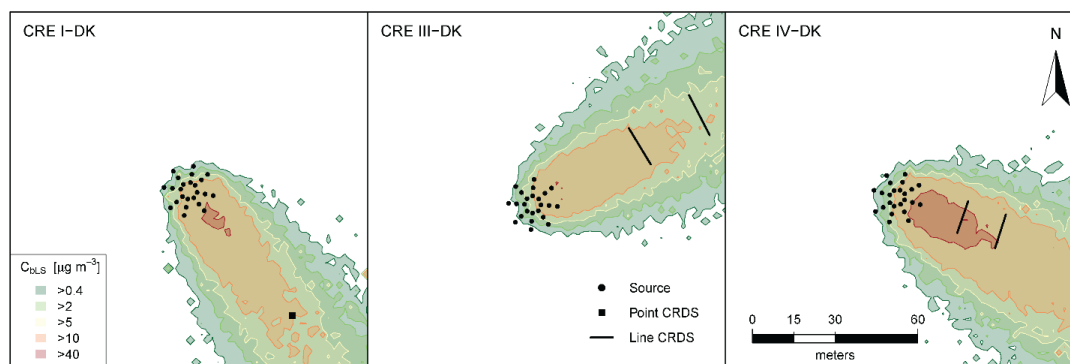
351

352 *Figure 5 .- Ammonia (NH_3) fluxes measured with Line 2 and Line 3 in 10 min intervals average in VIII-*
353 *DK.*

354 The point CRDS system had a recovery rate of 0.70 ± 0.22 and 1.01 ± 0.05 for NH_3 and CH_4 ,
355 respectively. The benefit of the point CRDS system is mainly that increasing the flow in the tubing is less
356 limited, since there are no critical orifices for which equal flow must be maintained. However, comparing
357 point and line CRDS systems by the modelled concentration distribution (Figure 6), the line-integrated
358 measurement system covers a larger part of the emission plume from the source in a higher wind direction
359 range. In addition, a line-integrated measurement system can reduce uncertainty in the IDM (Flesch et al.,
360 2004), since it is less sensitive to error in the measured wind direction. This is in accordance with Ro et
361 al. (2011), who observed an almost double recovery value of a line-integrated measurement system for
362 CH_4 compared to a point measurement system using a photoacoustic gas monitor.



363



364 *Figure 6.- Contours of the modelled concentration distribution (C_{bLS}) for CRE I-DK, CRE III-DK and*
365 *CRE IV-DK.*

366 3.3 Open-path measurement systems

367 The recovery rates for the GFs (CH_4) ranged from 0.87 ± 0.10 to 1.08 ± 0.15 . In V-CH to VII-CH,
368 the corresponding standard deviation $\sigma_{Q_{bLS}/Q}$ of GF 15 m varies from 0.07 to 0.18, while Line 1 (placed
369 parallel to GF 15 m) ranges from 0.06 to 0.10. These standard deviations $\sigma_{Q_{bLS}/Q}$ are comparable with
370 those measured by Gao et al. (2009) (1.03 ± 0.16).

371 In V-CH and VI-CH (source at ground), the MDs (NH_3) had recovery rates ranging from $0.57 \pm$
372 0.12 to 0.93 ± 0.03 . In VII-CH, MDs exhibit higher recoveries ranging from 0.64 ± 0.09 to 0.98 ± 0.10
373 since the source was elevated. Generally, it is recommended to do a release experiment above ground
374 level to reduce the probability of deposition close to the release area (McBain and Desjardins, 2005b). As
375 expected, the recovery rate decreased with downwind distance of the sampling position due to NH_3
376 deposition, which will be evaluated in section 3.4. Comparing MD at 15 m and Line 1 (placed in parallel)
377 in V-CH to VII-CH (Figure 2), the recovery rates are higher for MD. The highest difference between MD
378 and Line 1 was in V-CH, where there were the highest RH (87%). However, there are no clear patterns
379 explaining the difference between emissions from the different measurement systems based on
380 atmospheric conditions (Supplementary information, Figure S2). Although, the improved recovery with
381 Line 2 (0.81 ± 0.16) and Line 3 (0.87 ± 0.11) in IV-DK and VIII-DK could be influenced by the warmer



382 conditions and solar radiation (Table 2), it is plausible that the line improvements caused the increase. An
383 increased flow through the orifices and higher temperature of the sampling line will lead to less NH₃
384 adsorption thereby getting a better recovery from the release.

385 This results show the advantage of an open-path instrument compared to a closed-path instrument
386 to measure NH₃ emissions (Figure 2), since open-path avoids prolonged response caused by the
387 adsorption of NH₃ to sampling materials (Shah et al., 2006; Vaittinen et al., 2014). However, it is more
388 difficult to evaluate the quality of measurements by an open-path instrument due to complexity of the
389 calibration that depends on the path length between the sensor and reflector (DeBruyn et al., 2020) or the
390 need of another instrument for intercomparison (Häni et al., 2021). In addition, the closed-path system
391 presented in this study (line CRDS) is more flexible with respect to moving the sampling line around the
392 source depending on the predominant wind direction. This factor has different impact in different
393 countries, e.g. in the case in Denmark wind direction change quite more often than in Switzerland.

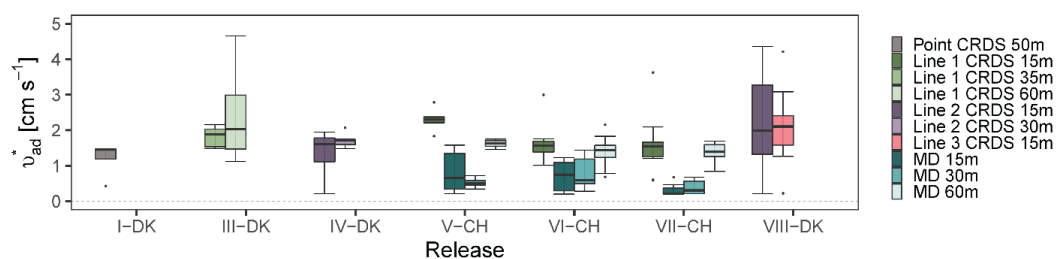
394 3.4 Surface deposition velocity

395 The corresponding surface deposition velocities (v_{ad}^*) required to have a recovery rate $Q_{bLS}/Q = 1$
396 are presented in Figure 7. This approach assumes a complete recovery for each of the measurement
397 systems when taking deposition into account, which is not completely correct for closed-path sampling.
398 In the following, therefore, we refer to deposition velocity required to achieve $Q_{bLS}/Q = 1$ as the *apparent*
399 deposition velocity (v_{ad}^*). This is included to provide data on deposition velocities for ammonia for which
400 data is currently very limited. The recovery rates observed in Figure 3 show that the MD performed best,
401 whereas lower Q_{bLS}/Q were seen in the sampling lines, thus the lowest v_{ad}^* is expected from MD.
402 Additional information of R_c and v_{ad}^* for each time intervals in each experiment is shown in Table S1 in
403 the Supplementary Information. The apparent surface deposition velocities ranged from 0.2 to 2.2 cm s⁻¹
404 for open-path data and from 0.2 to 4.7 cm s⁻¹ for the line sampling, respectively. Häni et al. (2018)
405 reported v_{ad}^* in the range from 0.3 to 1.1 cm s⁻¹. In all the releases where downwind concentrations were



406 measured at different positions, v_{ad}^* appears to increase with distance increases, with many cases. For
407 example, in VI-CH, v_{ad}^* is 0.7 ± 0.4 , 0.8 ± 0.4 and 1.4 ± 0.4 cm s^{-1} at 15 m, 30 m and 60 m, respectively.
408 This is in line with the outcome of Asman and van Jaarsveld. (1991); a significant fraction of the emitted
409 NH_3 is deposited near the source, which supports the regulations that do not allow livestock sources near
410 sensitive eutrophic ecosystems (NEC Directive 2016/2284).

411 In V-CH, VI-CH and VII-CH, v_{ad}^* from Line 1 are 2.8, 2.2 and 5.1 times higher than MD at 15 m.
412 As expected v_{ad}^* was higher for Line 1 as the Q/Q was lower for Line 1 compared to MD in these
413 experiments. Line 1 (VII-CH) had v_{ad}^* of 1.6 ± 0.9 , whereas Line 2 and Line 3 (VIII-DK) had v_{ad}^* of 2.2
414 ± 1.4 and 2.1 ± 1.0 cm s^{-1} , respectively, when measuring 15 m from the elevated source. During VII-CH
415 and VIII-DK the temperature differed 1°C and the relative humidity was approximately the same, but
416 wind speed and solar radiation differed (Table 2). However, comparing the apparent deposition velocities
417 from these experiments show comparable values for Lines 2 and 3, but higher values for Line 1. Overall,
418 the Q/Q values for Line 1 were worse than MD and Lines 2 and 3, which is reflected it in the higher
419 apparent deposition velocities.



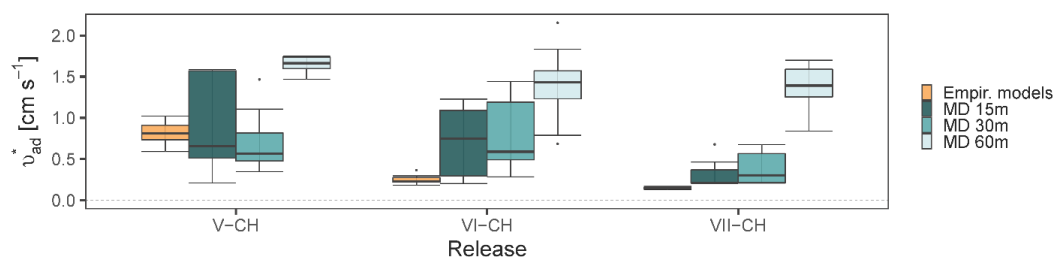
420

421 *Figure 7. - Corresponding apparent surface deposition velocities (v_{ad}^*) required to have a recovery rate*
422 *$Q_{bl,S}/Q$ closest to 1 in all the releases. All values are shown in Table S1 in the Supplementary Information.*

423 Many factors affect the deposition velocity, but it is possible to calculate v_{ad}^* from empirical
424 models as explained previously (see section 2.6). *Figure 8* shows v_{ad}^* for MDs in V-CH, VII-CH, and
425 VIII-CH compared to v_{ad}^* calculated with the empirical models (equations 3-8). Using the empirical
426 models, v_{ad}^* varies from 0.13 to 1.02 cm s^{-1} , increasing with the relative humidity (87%, 76% and 52%



427 RH in V-CH, VI-CH and VII-CH, respectively). The difference between the two ways of estimating v_{ad}^*
428 highlights the complexity and uncertainty for these methods. In addition, an artificial source has higher v_{ad}^*
429 than what is expected from a real agricultural source (Häni et al., 2018). This is seen with the higher v_{ad}^*
430 values found in these experiments compared to the calculated values with the empirical models. The
431 height of the source might also have an influence on v_{ad}^* . This is indicated by the lowest v_{ad}^* in VII-CH,
432 where the source was elevated compared to V-CH and VI-CH, where the gas was released on the surface.
433 Placing the source above ground level will reduce the obstacles (crop on the field) for gas dispersion,
434 reducing surface deposition. However, the bLS model does not consider the height of the source. For
435 example, evaluating emissions from the application of liquid animal manure (ground level source) or a
436 dairy housing (elevated source) will have different v_{ad}^* .



437

438 *Figure 8.- Corresponding apparent surface deposition velocities (v_{ad}^*) required to have a recovery*
439 *rate Q_{bLS}/Q closest to 1 for miniDOAS (MD) in release V-CH, VI-CH and VII-CH and v_{ad}^* calculated*
440 *with an empirical models.*

441

442 3.5 Sensitivity analysis

443 A sensitivity analysis of the bLS model was based on the resulting Q/Q ratio when changing the
444 inlet height of the analyzer and the wind direction offset compared to the valid measured values in release
445 VIII-DK. This was done for 11 fluxes average intervals of 15 min, where all emissions were estimated
446 again with the bLS model. For the assessment of the influence of the input for the measurement height all
447 other variables were kept constant. Likewise, for the influence of the wind direction, all other variables



448 were kept constant while the wind direction offset was changed. The results are presented in Figure S4 in
449 the Supplementary Information, where it can be seen that Q/Q was most sensitive to the changes in wind
450 direction offset, stressing the importance of the true offset in wind direction. Therefore, the wind direction
451 must be thoroughly evaluated for the accuracy of emission estimation since more or less trajectories have
452 touchdowns inside of the source area for the dispersion factor (Eq. 2). In addition, the uncertainty of Q/Q
453 ratio increases as wind direction offset increases. The emission estimation accuracy from point systems is
454 more sensitive to error in the measured wind direction (Flesch et al., 2004).

455 The accuracy of the emission estimation also depends on the detection limits of the concentration
456 sensor analyzer, especially when the downwind concentration is close to the background level, as it was
457 shown previously (see section 3.2). Therefore, it is recommended to conduct concentration and turbulence
458 measurements not far from the source but minimum 10 times the source height according to Harper et al.
459 (2011) at a known height to reduce the uncertainty of the calculated emissions rates.

460 **4 Conclusion**

461 Line-average concentration measurement with a closed-path analyzer is comparable with an open-
462 path system, as the average of all releases with all instrument types, the CH_4 recovery rate Q_{bLS}/Q was
463 0.95 ± 0.08 ($n = 19$). Under comparable conditions, an average NH_3 recovery rate of 0.82 ± 0.05 ($n = 3$)
464 and 0.91 ± 0.07 ($n = 3$) was obtained with the closed-path and open-path line integrated system,
465 respectively. The implementation of the new method presented in this study will enable measurement of
466 fluxes of multiple gases from different type of sources and evaluate the effects of mitigation strategies on
467 emissions. In addition, this method allows for continuous online measurements that resolve temporal
468 variation in NH_3 emissions and the peak emissions of CH_4 .

469 A significant fraction of the emitted NH_3 is deposited near the source. Consequently, including the
470 deposition algorithm in the bLS model will have a greater influence on the emission evaluation at ground
471 level sources (e.g. application of liquid animal manure), compared to elevated sources (e.g. slurry tank).



472 The present study shows that the deposition algorithm included in the bLS model estimates correct NH₃
473 emissions that considers surface deposition. In addition, the wind direction must be thoroughly evaluated
474 for the accuracy of emission estimation with the bLS model.

475 **Acknowledgments**

476 This study was funded by the Ministry of the Environment and Food of Denmark as a service
477 agreement 2019-760-001136. Thanks to Simon Bowald for his great ideas and his help with designing
478 and building up the Line 3. Also thanks to technicians Martin Häberli-Wyss, Peter Storegård Nielsen,
479 Jens Kristian Kristensen, and Heidi Grønbæk for their invaluable help during the experimental part of the
480 study.

481 **References**

- 482 Aneja, V.P., Schlesinger, W.H., Erisman, J.W., 2009. Effects of Agriculture upon the Air Quality
483 and Climate: Research, Policy, and Regulations. *Environmental Science & Technology* 43,
484 4234–4240. <https://doi.org/10.1021/es8024403>
- 485 Asman, W.A.H., van Jaarsveld, H.A., 1991. A variable-resolution transport model applied for
486 NH_x in Europe. *Atmospheric Environment* 445–464. [https://doi.org/10.1016/0960-](https://doi.org/10.1016/0960-1686(92)90329-J)
487 [1686\(92\)90329-J](https://doi.org/10.1016/0960-1686(92)90329-J)
- 488 Bai, M., Loh, Z., Griffith, D.W.T., Turner, D., Eckard, R., Edis, R., Denmead, O.T., Bryant,
489 G.W., Paton-Walsh, C., Tonini, M., McGinn, S.M., Chen, D., 2022. Performance of open-path
490 lasers and Fourier transform infrared spectroscopic systems in agriculture emissions research.
491 *Atmos. Meas. Tech.* 15, 3593–3610. <https://doi.org/10.5194/amt-15-3593-2022>
- 492 Baldé, H., VanderZaag, A.C., Burt, S., Evans, L., Wagner-Riddle, C., Desjardins, R.L.,
493 MacDonald, J.D., 2016a. Measured versus modeled methane emissions from separated liquid



- 494 dairy manure show large model underestimates. *Agriculture, Ecosystems & Environment* 230,
495 261–270. <https://doi.org/10.1016/j.agee.2016.06.016>
- 496 Baldé, H., VanderZaag, A.C., Burt, S.D., Wagner-Riddle, C., Crolla, A., Desjardins, R.L.,
497 MacDonald, D.J., 2016b. Methane emissions from digestate at an agricultural biogas plant.
498 *Bioresource Technology* 216, 914–922. <https://doi.org/10.1016/j.biortech.2016.06.031>
- 499 Baldé, H., VanderZaag, A.C., Burt, S.D., Wagner-Riddle, C., Evans, L., Gordon, R., Desjardins,
500 R.L., MacDonald, J.D., 2018. Ammonia emissions from liquid manure storages are affected by
501 anaerobic digestion and solid-liquid separation. *Agricultural and Forest Meteorology* 258, 80–88.
502 <https://doi.org/10.1016/j.agrformet.2018.01.036>
- 503 Baldocchi, D.D., Hicks, B.B., Camara, P., 1987. A canopy stomatal resistance model for gaseous
504 deposition to vegetated surfaces. *Atmospheric Environment* (1967) 21, 91–101.
505 [https://doi.org/10.1016/0004-6981\(87\)90274-5](https://doi.org/10.1016/0004-6981(87)90274-5)
- 506 Bühler, M., Häni, C., Ammann, C., Mohn, J., Neftel, A., Schrade, S., Zähler, M., Zeyer, K.,
507 Brönnimann, S., Kupper, T., 2021. Assessment of the inverse dispersion method for the
508 determination of methane emissions from a dairy housing. *Agricultural and Forest Meteorology*
509 307, 108501. <https://doi.org/10.1016/j.agrformet.2021.108501>
- 510 Carozzi, M., Loubet, B., Acutis, M., Rana, G., Ferrara, R.M., 2013. Inverse dispersion modelling
511 highlights the efficiency of slurry injection to reduce ammonia losses by agriculture in the Po
512 Valley (Italy). *Agricultural and Forest Meteorology* 171–172, 306–318.
513 <https://doi.org/10.1016/j.agrformet.2012.12.012>



- 514 Coates, T.W., Alam, M., Flesch, T.K., Hernandez-Ramirez, G., 2021. Field testing two flux
515 footprint models. *Atmos. Meas. Tech.* 14, 7147–7152. <https://doi.org/10.5194/amt-14-7147-2021>
- 516 DeBruyn, Z.J., Wagner-Riddle, C., VanderZaag, A., 2020. Assessment of Open-path
517 Spectrometer Accuracy at Low Path-integrated Methane Concentrations. *Atmosphere* 11, 184.
518 <https://doi.org/10.3390/atmos11020184>
- 519 Delre, A., Mønster, J., Samuelsson, J., Fredenslund, A.M., Scheutz, C., 2018. Emission
520 quantification using the tracer gas dispersion method: The influence of instrument, tracer gas
521 species and source simulation. *Science of The Total Environment* 634, 59–66.
522 <https://doi.org/10.1016/j.scitotenv.2018.03.289>
- 523 Desjardins, R.L., Denmead, O.T., Harper, L., McBain, M., Massé, D., Kaharabata, S., 2004.
524 Evaluation of a micrometeorological mass balance method employing an open-path laser for
525 measuring methane emissions. *Atmospheric Environment* 38, 6855–6866.
526 <https://doi.org/10.1016/j.atmosenv.2004.09.008>
- 527 EEA, 2019. EMEP/EEA air pollutant emission inventory guidebook 2019: technical guidance to
528 prepare national emission inventories. Publications Office, LU.
- 529 FAO, 2017. Food and Agriculture Organization of the United Nations. The future of food and
530 agriculture: trends and challenges. Food and Agriculture Organization of the United Nations,
531 Rome.
- 532 Flesch, T., Wilson, J., Harper, L., Crenna, B., 2005. Estimating gas emissions from a farm with
533 an inverse-dispersion technique. *Atmospheric Environment* 39, 4863–4874.
534 <https://doi.org/10.1016/j.atmosenv.2005.04.032>



- 535 Flesch, T.K., Desjardins, R.L., Worth, D., 2011. Fugitive methane emissions from an agricultural
536 biodigester. *Biomass and Bioenergy* 35, 3927–3935.
537 <https://doi.org/10.1016/j.biombioe.2011.06.009>
- 538 Flesch, T.K., McGinn, S.M., Chen, D., Wilson, J.D., Desjardins, R.L., 2014. Data filtering for
539 inverse dispersion emission calculations. *Agricultural and Forest Meteorology* 198–199, 1–6.
540 <https://doi.org/10.1016/j.agrformet.2014.07.010>
- 541 Flesch, T.K., Wilson, J.D., Harper, L.A., Crenna, B.P., Sharpe, R.R., 2004. Deducing Ground-to-
542 Air Emissions from Observed Trace Gas Concentrations: A Field Trial. *Journal of Applied*
543 *Meteorology* 43, 487–502. <https://doi.org/10.1175/JAM2214.1>
- 544 Flesch, T.K., Wilson, J.D., Harper, L.A., Todd, R.W., Cole, N.A., 2007. Determining ammonia
545 emissions from a cattle feedlot with an inverse dispersion technique. *Agricultural and Forest*
546 *Meteorology* 144, 139–155. <https://doi.org/10.1016/j.agrformet.2007.02.006>
- 547 Flesch, T.K., Wilson, J.D., Yee, E., 1995. Backward-Time Lagrangian Stochastic Dispersion
548 Model and Their Application to Estimate Gaseous Emissions. *Journal of Applied Meteorology*
549 34, 1320–1332. <https://doi.org/10.1175/1520-0450>
- 550 Fredenslund, A.M., Rees-White, T.C., Beaven, R.P., Delre, A., Finlayson, A., Helmore, J., Allen,
551 G., Scheutz, C., 2019. Validation and error assessment of the mobile tracer gas dispersion
552 method for measurement of fugitive emissions from area sources. *Waste Management* 83, 68–78.
553 <https://doi.org/10.1016/j.wasman.2018.10.036>
- 554 Gao, Z., Desjardins, R.L., Flesch, T.K., 2009. Comparison of a simplified micrometeorological
555 mass difference technique and an inverse dispersion technique for estimating methane emissions



- 556 from small area sources. *Agricultural and Forest Meteorology* 149, 891–898.
557 <https://doi.org/10.1016/j.agrformet.2008.11.005>
- 558 Gao, Z., Desjardins, R.L., van Haarlem, R.P., Flesch, T.K., 2008. Estimating Gas Emissions
559 from Multiple Sources Using a Backward Lagrangian Stochastic Model. *Journal of the Air &*
560 *Waste Management Association* 58, 1415–1421. <https://doi.org/10.3155/1047-3289.58.11.1415>
- 561 Garland, J.A., 1977. The dry deposition of sulphur dioxide to land and water surfaces. *Proc. R.*
562 *Soc. Lond. A* 354, 245–268. <https://doi.org/10.1098/rspa.1977.0066>
- 563 Grant, R.H., Boehm, M.T., Bogan, B.W., 2015. Methane and carbon dioxide emissions from
564 manure storage facilities at two free-stall dairies. *Agricultural and Forest Meteorology* 213, 102–
565 113. <https://doi.org/10.1016/j.agrformet.2015.06.008>
- 566 Hafner, S.D., 2018. The ALFAM2 database on ammonia emission from field-applied manure_
567 Description and illustrative analysis. *Agricultural and Forest Meteorology* 14.
- 568 Häni, C., Bühler, M., Neftel, A., Ammann, C., Kupper, T., 2021. Performance of open-path
569 GasFinder3 devices for CH₄ concentration measurements close to
570 ambient levels. *Atmos. Meas. Tech.* 14, 1733–1741. <https://doi.org/10.5194/amt-14-1733-2021>
- 571 Häni, C., Flechard, C., Neftel, A., Sintermann, J., Kupper, T., 2018. Accounting for Field-Scale
572 Dry Deposition in Backward Lagrangian Stochastic Dispersion Modelling of NH₃ Emissions.
573 <https://doi.org/10.20944/preprints201803.0026.v1>
- 574 Harper, L.A., Denmead, O.T., Flesch, T.K., 2011. Micrometeorological techniques for
575 measurement of enteric greenhouse gas emissions. *Animal Feed Science and Technology* 166–
576 167, 227–239. <https://doi.org/10.1016/j.anifeedsci.2011.04.013>



- 577 Harper, L.A., Flesch, T.K., Powell, J.M., Coblenz, W.K., Jokela, W.E., Martin, N.P., 2009.
578 Ammonia emissions from dairy production in Wisconsin. *Journal of Dairy Science* 92, 2326–
579 2337. <https://doi.org/10.3168/jds.2008-1753>
- 580 Harper, L.A., Flesch, T.K., Weaver, K.H., Wilson, J.D., 2010. The Effect of Biofuel Production
581 on Swine Farm Methane and Ammonia Emissions. *Environmental Quality* 39, 1984–1992.
582 <https://doi.org/10.2134/jeq2010.0172>
- 583 Hu, E., Babcock, E.L., Bialkowski, S.E., Jones, S.B., Tuller, M., 2014. Methods and Techniques
584 for Measuring Gas Emissions from Agricultural and Animal Feeding Operations. *Critical*
585 *Reviews in Analytical Chemistry* 44, 200–219. <https://doi.org/10.1080/10408347.2013.843055>
- 586 Hu, N., Flesch, T.K., Wilson, J.D., Baron, V.S., Basarab, J.A., 2016. Refining an inverse
587 dispersion method to quantify gas sources on rolling terrain. *Agricultural and Forest*
588 *Meteorology* 225, 1–7. <https://doi.org/10.1016/j.agrformet.2016.05.007>
- 589 Kamp, J.N., Chowdhury, A., Adamsen, A.P.S., Feilberg, A., 2019. Negligible influence of
590 livestock contaminants and sampling system on ammonia measurements with cavity ring-down
591 spectroscopy. *Measurement Techniques* 12, 2837–2850. [https://doi.org/10.5194/amt-12-2837-](https://doi.org/10.5194/amt-12-2837-2019)
592 2019
- 593 Kamp, J.N., Häni, C., Nyord, T., Feilberg, A., Sørensen, L.L., 2021. Calculation of NH₃
594 Emissions, Evaluation of Backward Lagrangian Stochastic Dispersion Model and Aerodynamic
595 Gradient Method 17.
- 596 Kupper, T., Eugster, R., Sintermann, J., Häni, C., 2021. Ammonia emissions from an uncovered
597 dairy slurry storage tank over two years: Interactions with tank operations and meteorological



- 598 conditions. *Biosystems Engineering* 204, 36–49.
- 599 <https://doi.org/10.1016/j.biosystemseng.2021.01.001>
- 600 Lemes, Y.M., Garcia, P., Nyord, T., Feilberg, A., Kamp, J.N., 2022. Full-scale investigation of
601 methane and ammonia mitigation by early single-dose slurry storage acidification [Submitted
602 June 2022].
- 603 Lynn, B.H., Carlson, T.N., 1990. A stomatal resistance model illustrating plant vs. external
604 control of transpiration. *Agricultural and Forest Meteorology* 52, 5–43.
- 605 [https://doi.org/10.1016/0168-1923\(90\)90099-R](https://doi.org/10.1016/0168-1923(90)90099-R)
- 606 Massad, R.-S., Nemitz, E., Sutton, M.A., 2010. Review and parameterisation of bi-directional
607 ammonia exchange between vegetation and the atmosphere. *Atmos. Chem. Phys.* 10, 10359–
608 10386. <https://doi.org/10.5194/acp-10-10359-2010>
- 609 McBain, M.C., Desjardins, R.L., 2005a. The evaluation of a backward Lagrangian stochastic
610 (bLS) model to estimate greenhouse gas emissions from agricultural sources using a synthetic
611 tracer source. *Agricultural and Forest Meteorology* 135, 61–72.
- 612 <https://doi.org/10.1016/j.agrformet.2005.10.003>
- 613 McBain, M.C., Desjardins, R.L., 2005b. The evaluation of a backward Lagrangian stochastic
614 (bLS) model to estimate greenhouse gas emissions from agricultural sources using a synthetic
615 tracer source. *Agricultural and Forest Meteorology* 135, 61–72.
- 616 <https://doi.org/10.1016/j.agrformet.2005.10.003>



- 617 McGinn, S.M., Coates, T., Flesch, T.K., Crenna, B., 2008. Ammonia emission from dairy cow
618 manure stored in a lagoon over summer. *Can. J. Soil. Sci.* 88, 611–615.
619 <https://doi.org/10.4141/CJSS08002>
- 620 McGinn, S.M., Flesch, T.K., Beauchemin, K.A., Shreck, A., Kindermann, M., 2019.
621 *Micrometeorological Methods for Measuring Methane Emission Reduction at Beef Cattle*
622 *Feedlots: Evaluation of 3-Nitrooxypropanol Feed Additive. J. environ. qual.* 48, 1454–1461.
623 <https://doi.org/10.2134/jeq2018.11.0412>
- 624 McGinn, S.M., Flesch, T.K., Crenna, B.P., Beauchemin, K.A., Coates, T., 2007. Quantifying
625 Ammonia Emissions from a Cattle Feedlot using a Dispersion Model. *J. Environ. Qual.* 36,
626 1585–1590. <https://doi.org/10.2134/jeq2007.0167>
- 627 McGinn, S.M., Turner, D., Tomkins, N., Charmley, E., Bishop-Hurley, G., Chen, D., 2011.
628 *Methane Emissions from Grazing Cattle Using Point-Source Dispersion. J. Environ. Qual.* 40,
629 22–27. <https://doi.org/10.2134/jeq2010.0239>
- 630 NEC Directive 2016/2284, n.d. DIRECTIVE (EU) 2016/ 2284 OF THE EUROPEAN
631 PARLIAMENT AND OF THE COUNCIL - of 14 December 2016 - on the reduction of
632 national emissions of certain atmospheric pollutants, amending Directive 2003/ 35/ EC
633 and repealing Directive 2001/ 81/ EC.
- 634 OECD, FAO, 2019. *OECD-FAO Agricultural Outlook 2019-2028*, OECD-FAO Agricultural
635 Outlook. OECD. https://doi.org/10.1787/agr_outlook-2019-en



- 636 Pedersen, J.M., Feilberg, A., Kamp, J.N., Hafner, S., Nyord, T., 2020. Ammonia emission
637 measurement with an online wind tunnel system for evaluation of manure application techniques.
638 Atmospheric Environment 230, 117562. <https://doi.org/10.1016/j.atmosenv.2020.117562>
- 639 Platt, U., Stutz, J., 2008. Differential optical absorption spectroscopy: principles and
640 applications, Physics of Earth and space environments. Springer, Berlin.
- 641 R Core Team, 2018. R: A language and environment for statistical computing; R Foundation for
642 Statistical. Computing: Vienna, Austria.
- 643 Ro, K.S., Johnson, M.H., Hunt, P.G., Flesch, T.K., 2011. Measuring Trace Gas Emission from
644 Multi-Distributed Sources Using Vertical Radial Plume Mapping (VRPM) and Backward
645 Lagrangian Stochastic (bLS) Techniques. Atmosphere 2, 553–566.
646 <https://doi.org/10.3390/atmos2030553>
- 647 Ro, K.S., Stone, K.C., Johnson, M.H., Hunt, P.G., Flesch, T.K., Todd, R.W., 2014. Optimal
648 Sensor Locations for the Backward Lagrangian Stochastic Technique in Measuring Lagoon Gas
649 Emission. Journal of Environmental Quality 43, 1111–1118.
650 <https://doi.org/10.2134/jeq2013.05.0163>
- 651 Sanz, A., Misselbrook, T., Sanz, M.J., Vallejo, A., 2010. Use of an inverse dispersion technique
652 for estimating ammonia emission from surface-applied slurry. Atmospheric Environment 44,
653 999–1002. <https://doi.org/10.1016/j.atmosenv.2009.08.044>
- 654 Shah, S.B., Grabow, G.L., Westerman, P.W., 2006. Ammonia Adsorption in Five Types of
655 Flexible Tubing Materials. Applied Engineering in Agriculture 22, 919–923.
656 <https://doi.org/10.13031/2013.22253>



- 657 Sintermann, J., Ammann, C., Kuhn, U., Spirig, C., Hirschberger, R., Gärtner, A., Neftel, A.,
658 2011. Determination of field scale ammonia emissions for common slurry spreading practice
659 with two independent methods. *Atmospheric Measurement Techniques* 4, 1821–1840.
660 <https://doi.org/10.5194/amt-4-1821-2011>
- 661 Sintermann, J., Dietrich, K., Häni, C., Bell, M., Jocher, M., Neftel, A., 2016. A miniDOAS
662 instrument optimised for ammonia field measurements. *Atmospheric Measurement Techniques*
663 9, 2721–2734. <https://doi.org/10.5194/amt-9-2721-2016>
- 664 Sommer, S.G., McGinn, S.M., Hao, X., Larney, F.J., 2004. Techniques for measuring gas
665 emissions from a composting stockpile of cattle manure. *Atmospheric Environment* 38, 4643–
666 4652. <https://doi.org/10.1016/j.atmosenv.2004.05.014>
- 667 Todd, R.W., Cole, N.A., Rhoades, M.B., Parker, D.B., Casey, K.D., 2011. Daily, Monthly,
668 Seasonal, and Annual Ammonia Emissions from Southern High Plains Cattle Feedyards. *J.*
669 *Environ. Qual.* 40, 1090–1095. <https://doi.org/10.2134/jeq2010.0307>
- 670 Vaittinen, O., Metsälä, M., Persijn, S., Vainio, M., Halonen, L., 2014. Adsorption of ammonia on
671 treated stainless steel and polymer surfaces. *Applied Physics B* 115, 185–196.
672 <https://doi.org/10.1007/s00340-013-5590-3>
- 673 van Haarlem, R.P., Desjardins, R.L., Gao, Z., Flesch, T.K., Li, X., 2008. Methane and ammonia
674 emissions from a beef feedlot in western Canada for a twelve-day period in the fall. *Can. J.*
675 *Anim. Sci.* 88, 641–649. <https://doi.org/10.4141/CJAS08034>
- 676 VanderZaag, A.C., Flesch, T.K., Desjardins, R.L., Baldé, H., Wright, T., 2014. Measuring
677 methane emissions from two dairy farms: Seasonal and manure-management effects.



- 678 Agricultural and Forest Meteorology 194, 259–267.
679 <https://doi.org/10.1016/j.agrformet.2014.02.003>
- 680 Vechi, N.T., Mellqvist, J., Scheutz, C., 2022. Quantification of methane emissions from cattle
681 farms, using the tracer gas dispersion method. Agriculture, Ecosystems & Environment 330,
682 107885. <https://doi.org/10.1016/j.agee.2022.107885>
- 683 Voglmeier, K., Jocher, M., Häni, C., Ammann, C., 2018. Ammonia emission measurements of
684 an intensively grazed pasture. Biogeosciences 15, 4593–4608. [https://doi.org/10.5194/bg-15-](https://doi.org/10.5194/bg-15-4593-2018)
685 4593-2018
- 686 Wesely, M., 2007. Parameterization of surface resistances to gaseous dry deposition in regional-
687 scale numerical models☆. Atmospheric Environment 41, 52–63.
688 <https://doi.org/10.1016/j.atmosenv.2007.10.058>
- 689 Wilson, J.D., Flesch, T.K., Harper, L.A., 2001. Micro-meteorological methods for estimating
690 surface exchange with a disturbed windflow. Agricultural and Forest Meteorology 107, 207–225.
691 [https://doi.org/10.1016/S0168-1923\(00\)00238-0](https://doi.org/10.1016/S0168-1923(00)00238-0)
- 692 Yang, W., Que, H., Wang, S., Zhu, A., Zhang, Y., He, Y., Xin, X., Zhang, X., 2019. Comparison
693 of backward Lagrangian stochastic model with micrometeorological mass balance method for
694 measuring ammonia emissions from rice field. Atmospheric Environment 211, 268–273.
695 <https://doi.org/10.1016/j.atmosenv.2019.05.028>
- 696